論文

INITIATION AND PROPAGATION OF CRACKS DUE TO SIMULATED CORROSION OF REINFORCEMENT IN CONCRETE

Farid UDDIN A.K.M.*[1], Kenichiro NUMATA*[2], and Masayasu OHTSU*[3]

ABSTRACT: A detailed study on governing factors of initiation and propagation of cracks due to corrosion of reinforcement in concrete is performed. Due to expansion of corrosive products, cracks are nucleated around reinforcement in concrete. Initiation and propagation of cracks are studied experimentally and analytically. Numerical analysis by the boundary element method is conducted, on the basis of linear elastic fracture mechanics. The dimensionless stress intensity factors and the cracking modes are studied for two different types of crack patterns due to corrosion. It is confirmed that cracking mechanisms due to corrosion of reinforcement are dominantly associated with the mode-I failure.

KEYWORDS: corrosion of reinforcement, crack initiation and propagation, boundary element method (BEM), dimensionless stress intensity factor

1. INTRODUCTION

Concrete structures suffer reinforcement corrosion due to severe environments. This corrosion may lead into serious damages. So far, advances have been made in the inspection of deteriorated structures and the identification of cracking mechanisms due to corrosion of reinforcement. Most deteriorations of concrete can be attributed to corrosion of reinforcement. For making decision on maintenance and repair in reinforcement concrete, consequently, identification of cracking mechanisms due to corrosion is significantly important. Expansion caused by corrosion product generates cracking, of which mechanisms are investigated analytically by boundary element method (BEM)[1]. The maximum circumferential stress criterion based on linear elastic fracture mechanics (LEFM) was successfully applied to trace the crack extension. By employing the two-domain Boundary Element Method (BEM), crack orientations were evaluated from the stress intensity factors [2]. In the present paper, the two-domain BEM model is applied to investigate crack propagation due to rebar corrosion. For early warning of corrosion, nondestructive testing (NDT) is available. It is confirmed that corrosion potential on the reinforcement could be estimated by an improved half-cell potential measurement [3]. This implies that the zone of intense corrosion product can be located by NDT. Provided that pressure distribution due to expansion of corrosion products is reasonably assumed, prediction of crack propagation in concrete is readily performed prior to corrosion damage.

In order to develop an integrated procedure for predicting of crack initiation and propagation with NDT, crack extension in concrete due to corrosion product is studied, by applying LEFM and BEM. A systematic study is performed to clarify two types cracking mechanisms due to corrosion. Thus, theoretical models analyzed by two-domain BEM are applied to trace crack patterns which were observed in experiments.

*1Ph.D Student, Graduate School of Science and Technology, Kumamoto University, Member of JCI
*2Undergraduate Student, Department of Civil Engineering and Architecture, Kumamoto University
*3 Professor, Graduate School of Science and Technology, Kumamoto University, Dr. E., Member of JCI

2. EXPERIMENTS

To study crack patterns due to rebar corrosion in concrete, experiments were carried out. Concrete specimens of dimensions 25 x 25 x 10cm were tested. Concrete was made up of mixture as water (W): cement (C): sand (S): gravel (G) = 0.5: 1.0:2.41:2.95 by weight. The maximum size of aggregate was 20mm. Slump value and air content were 7.0cm and 5.0%, respectively. By making the concrete specimen an expansion test was conducted. Mechanical properties are obtained from cylindrical specimens at the age of 28days. Compressive strength at the 28days was 37.9MPa. Young's modulus of elasticity and Poisson's ratio are 29.7GPa and 0.22, respectively, which are employed in the BEM analysis.

Two types of concrete specimens 1 and 2 were prepared with cover thicknesses 4cm and 3cm, respectively. To investigate other types of cracks than the surface crack, a notch was created from the nearest side to the hole as shown in **Figs**. **1** and **2**. This is because the surface crack is definitely nucleated prior to other cracks[2]. Cracks due to corrosion of reinforcements are generated in the long process and very difficult to examine in the short time. Thus, expansion pressure was introduced by employing expansive agent.

In the figures, a circle of 3cm diameter represents the location of the reinforcement where the expansion pressure is applied by dolomite paste. In the experiments, the expansion pressure that creates cracking in concrete specimen was successfully measured by using a pressure gauge embedded at the center of the hole in depth. Observed cracks after experiments are also shown in **Figs.1** and **2**.

In specimen 1, the spalling crack Sc, and diagonal crack D are observed. In the case of specimen 2, the spalling crack Sc1, and the diagonal cracks D1 and D2 are observed. These two cracks of the spalling crack Sc and the diagonal crack D1 are investigated numerically as representative cracks in these specimens.

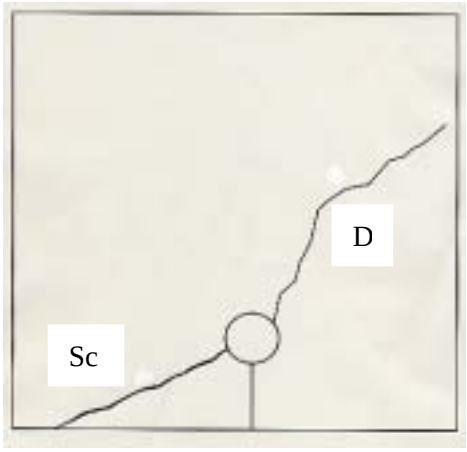

Fig.1 Observed cracks in specimen 1 (cover thickness 4cm).

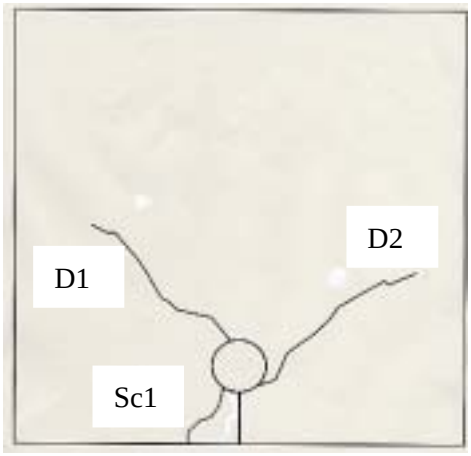

Fig.2 Observed cracks in specimen 2 (cover thickness 3cm).

3. ANALYTICALY MODEL

Analytical models for tracing the spalling crack Sc and the diagonal crack D1 are analyzed by BEM in a similar manner to the previous research[2]. Only a half portion of the specimen is considered for the analysis. This is because each crack path was nucleated in order[2]. Initial two-domain elements are stitched at the interface between the initial crack tip and the final point. All boundary meshes are of 5mm long. The effect of mesh sizes and the final point on the numerical accuracy was previous studied[4]. It is found that the accuracy of solutions is insensitive to the mesh division in the elastic problems. In the case of the two-domain BEM, however, the mesh size of the interfaces should be identical to that of the boundary element, in order to increase the accuracy. Based on these findings, the size of 5mm mesh is selected for all elements in the present analysis. It is important to point out one remark concerning selection of common interface. To the best of the authors' knowledge, the original interface has to be taken

as close as possible to the final crack trace. In this respect, the straight line joining the crack tip from the crack initiation to the final point is taken as close as possible to the crack trace actually observed. Because expansive agent was employed in the experiment, three types of expansive pressure are taken into consideration to simulate the expansion of corrosive products. These are uniform pressure, horizontal pressure and vertical pressure. Hereinafter, horizontal pressure is defined as applied into the X-axis direction and vertical as applied into the Y-axis in each figure.

The stress intensity factors K_I (mode I) and K_{II} (mode II) at the crack tip are determined from Smith's one-point formulae[5]. K_I and K_{II} are determined from relative displacements at the crack-tip elements. At each step of the analysis, the stress intensity factors are computed. When a crack propagates, the node at the crack tip is separated into two nodes, creating two stress-free elements in the direction θ. The stitching interface is created, connecting the crack tip with the final point. Thus, a new crack is created automatically in an arbitrary direction. The direction of the maximum tangential stress θ is determined from the maximum circumferential stress by Erdogan-Sih criterion[6] as,

$$K_I \sin\theta + K_{II}(3\cos\theta - 1) = 0 \qquad (1)$$

$$\cos\frac{\theta}{2}\left[K_I \cos^2\left(\frac{\theta}{2}\right) - \frac{3}{2}K_{II}\sin\theta\right] = K_{IC} \qquad (2)$$

From Eqs.(1) and (2), contribution K_I and K_{II} to K_{IC} can be obtained as the dimensionless stress intensity factors (K_I/K_{IC}) and (K_{II}/K_{IC})[7],

$$\left.\begin{aligned}(K_I/K_{IC}) &= \{(1-3\cos\theta)/\sin\theta\}/\,[\cos^3(\theta/2)\ x \\ &\quad \{(1-3\cos\theta)/\sin\theta - 3/2\sin\theta/\cos^2(\theta/2)\}] \\ (K_{II}/K_{IC}) &= 1/\,[\cos^3(\theta/2)\ x \\ &\quad \{(1-3\cos\theta)/\sin\theta - 3/2\sin\theta/\cos^2(\theta/2)\}]\end{aligned}\right\} \qquad (3)$$

Where K_{IC} is the critical stress intensity factor and is determined in the previously studies[8].
By testing the same concrete mixture, it is found to be equal to 0.723MPa $m^{1/2}$.

The dimensionless stress intensity factors (K_I/K_{IC}) and (K_{II}/K_{IC}) with the variation of crack-propagation angle θ are plotted in **Fig.3**. These curves show that either mode I or mode II is dominant, depending on the crack-propagation angle θ. The mode I is dominant from θ=0° to θ=53° while mode II is dominant from θ=53° to θ=90°.

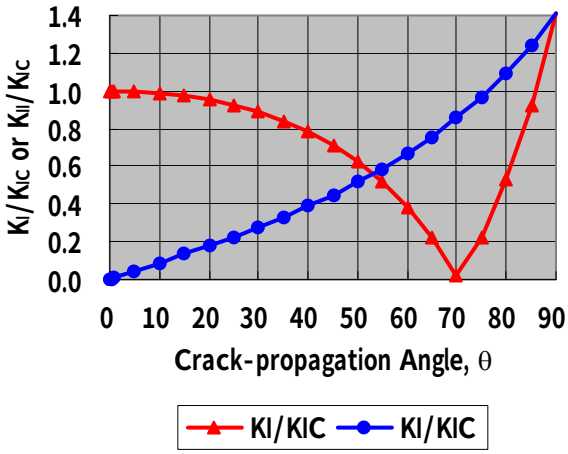

Fig.3 Dimensionless stress intensity factors with the variation of crack-propagation angle θ.

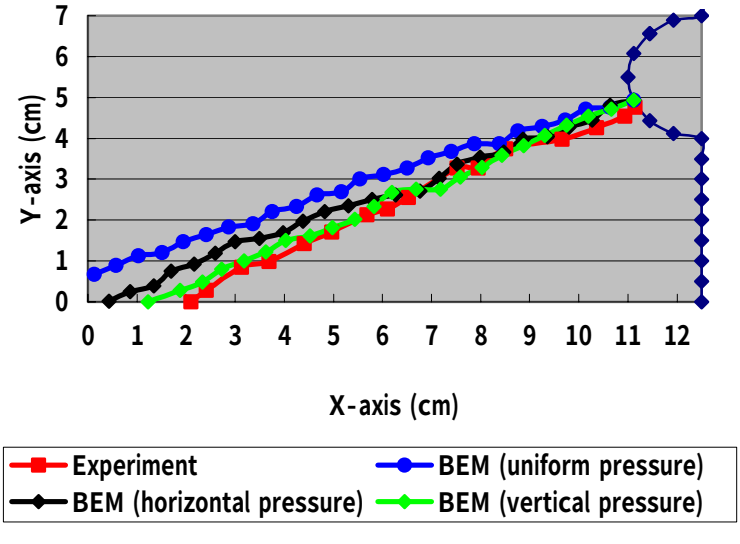

Fig.4 Crack traces by BEM for the spalling crack Sc.

4. MECHANISMS OF CRACK PROPAGATION

Observed crack patterns in the experiments are compared with those of BEM analysis, and the governing mechanisms are identified. Thus, each observed crack pattern is discussed as follows:

4.1 The Spalling crack (Sc)

The spalling crack Sc in specimen 1 is analyzed with the stress free boundary condition at the cover thickness. Crack trace by BEM is plotted along with the actual crack trace in the experiment in **Fig.4**. Here, only the left corner of the specimen is illustrated. Along the hole, uniform pressure, horizontal pressure, and vertical in the figure are taken into account. Through cracking steps, reasonable agreement between the actual crack trace in the experiment and those of BEM analysis is observed. From the beginning of crack extension, crack trace due to vertical pressure is closest to the actual trace in the experiment out of any other pressure distributions. This may imply that mechanisms of crack initiation and propagation for the spalling crack is directly involved with vertical pressure which corresponds to lateral movement at the hole in **Fig.1**. Based on the finding above, the pressure distributions for crack initiation and propagation are computed and shown in **Fig.5**.

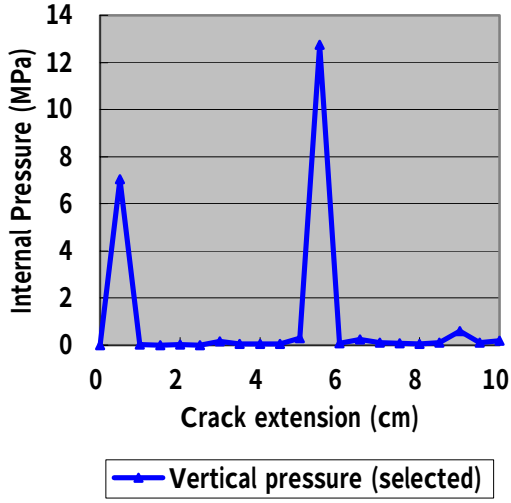

Fig.5 BEM simulation of the selected pressure for the spalling crack Sc.

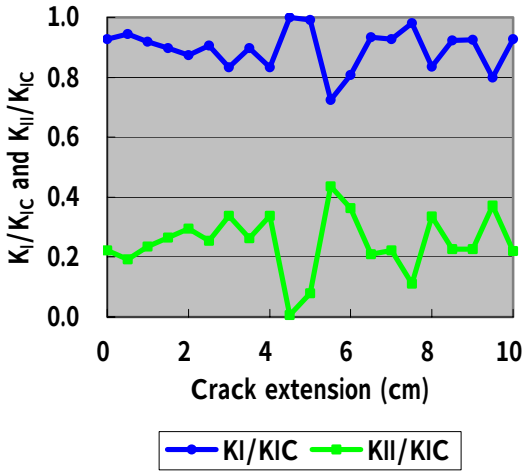

Fig.6 K_I/K_{IC} and K_{II}/K_{IC} during the crack extension of the spalling crack Sc.

The dimensionless stress intensity factors (K_I/K_{IC}) and (K_{II}/K_{IC}) are calculated at each step of crack extension by substituting crack-propagation angles in to Eq.(3). Results are given in **Fig.6**. In the beginning of crack extension, (K_I/K_{IC}) is nearly equal to 1.0, so the pure mode I fracture occurs. Although (K_{II}/K_{IC}) increases gradually, tensile crack is always dominant. As can be seen in **Fig.6**, at the middle stage of crack extension, contribution of K_{II} increases which may correspond to the increase of shear motion at the crack surface. From these results, it can be concluded that for propagation of the spalling crack Sc, tensile cracks eventually dominate shear cracks under extension.

4.2 The diagonal crack (D1)

The diagonal crack D1 in specimen 2 is analyzed with the stress free boundary condition at the cover thickness. Under the three kinds of pressure distributions, these crack traces are plotted along with on actual crack trace in the experiment as shown in **Fig.7**. Again, the left half of the specimen is illustrated here. From the beginning of crack propagation to 2.0cm crack extension, crack trace due to horizontal pressure is the closest to the actual trace, and from crack extension from 2.0 to final, that of uniform pressure is the closest. Based on these results possible pressure distributions under crack extension is reconstructed in **Fig.8**. The pressure distributions of eventually two peaks are observed.

The dimensionless stress intensity factors (K_I/K_{IC}) and (K_{II}/K_{IC}) are calculated at each step of crack extension by taking into account the angle of crack orientation in Eq.(3). Results are given in **Fig.9**. It is found that the mode I is also dominant in the diagonal crack. From the beginning of crack extension to the

final, (K_I/K_{IC}) is larger than 0.8, and so the mode I fracture is dominant. From **Fig.9** it is observed that the contribution of the mode II is increasing with crack extension while that of the mode II reaches the maximum around the middle of crack extension.

During the experiment, the internal pressure was measured. Although the internal expansion pressure was time dependent, simulated expansion pressures in BEM are not time-dependent. So, the actual internal pressure is not directly compared with the internal expansion pressures simulated by BEM. The pressure observed in the specimen 1 is given in **Fig.10**. The peak value reached is about 13MPa. From **Fig.5**, the peak value due to internal pressure for the spalling crack is about 13MPa. Thus, simulated internal pressure is in remarkable agreement with the actual expansion pressure. Observed pressure in specimen 2 is shown in **Fig.11**.

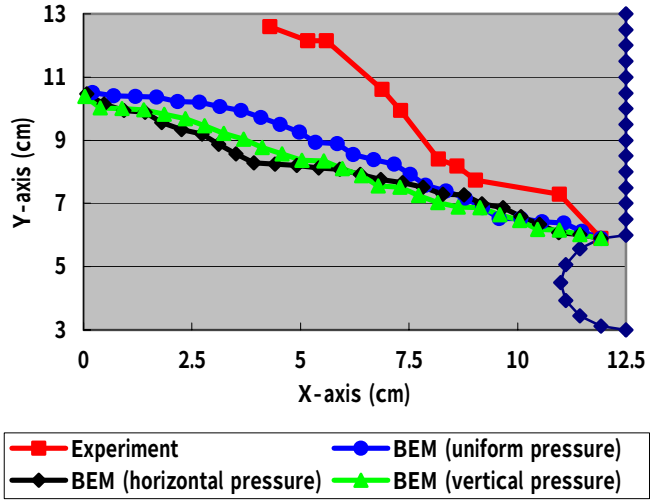

Fig. 7 Crack traces by BEM for the diagonal crack D1.

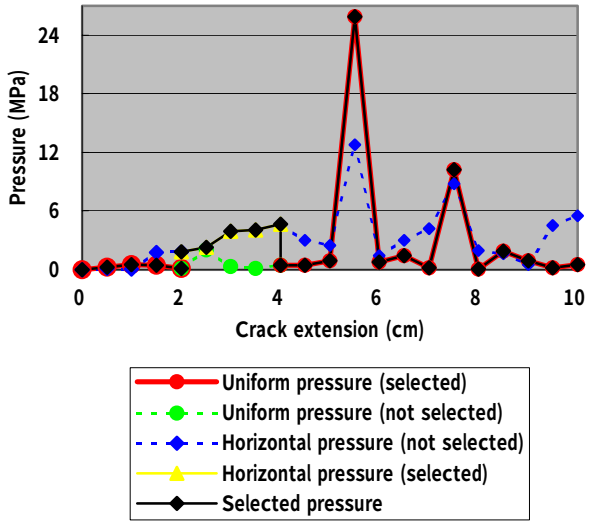

Fig.8 BEM simulation of the selected pressure for the diagonal crack D1.

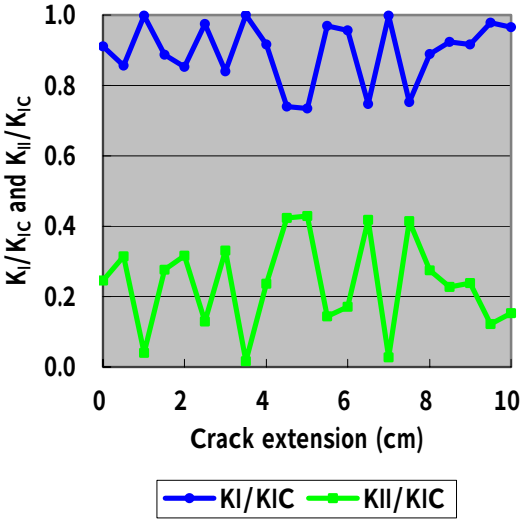

Fig.9 K_I/K_{IC} and K_{II}/K_{IC} during the crack extension of the diagonal crack D1.

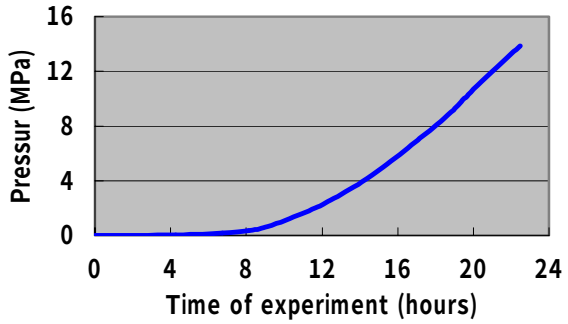

Fig.10 Internal pressure by experiment during the time of crack propagation in specimen 1.

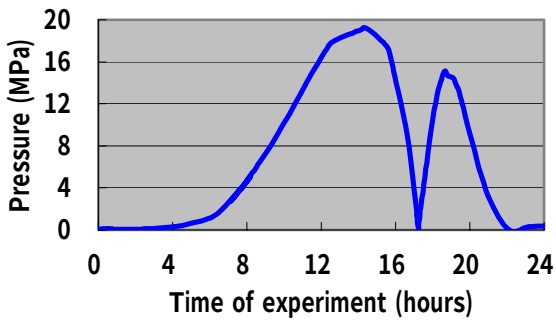

Fig.11 Internal pressure by experiment during the time of crack propagation in specimen 2.

From **Fig.11**, there exist two peaks. The first peak is about 19MPa and the second is about 15MPa. According to **Fig.8**, although two peaks are observed, the higher peak is about 24MPa. Thus, the simulated internal pressure of diagonal crack is higher than the actual internal pressure. This is probably because the simulated crack trace is a little far from the actual crack trace as shown in **Fig.7**.

Observed pressure in specimen 1 is lower than that of specimen 2, although the cover thickness of specimen 1 is thicker than specimen 2. It seems that cover thickness plays no significant role due to stress-free. Two diagonal cracks occurred in specimen 2, while only one diagonal crack in specimen 1. This suggests that more energy was released for propagating two diagonal cracks than one spalling crack. According to observation in experiments, the spalling crack started to propagate then others followed. More stable cracks for propagating were observed in specimen 2 than specimen 1. Thus, the pressure history of specimen 1 suddenly dropped earlier than specimen 2, creating the spalling crack in the brittle mode.

5. CONCLUSION

Crack initiation and propagation due to corrosion of reinforcement in concrete is studied numerically and experimentally. As a numerical technique, two-domain BEM is very promising for implementing the analysis of the mixed-mode discrete crack extension based on the maximum circumferential stress criterion. The method is readily applicable and allows simple automatic remeshing to model crack extension.

By applying the two-domain BEM, corrosion cracking in the arbitrary direction is automatically simulated on the spalling crack and the diagonal crack. The crack traces analyzed by BEM are in reasonable agreement with experimental results. Mechanisms of crack propagation due to corrosion of reinforcement are clarified by the dimensionless stress intensity factors (K_I/K_{IC} and K_{II}/K_{IC}) along with the crack extension. Concerning the mechanisms of crack propagation due to corrosion of reinforcement, mode-I is dominant in these two cracks.

REFERENCE

1. Ohtsu, M. and Yoshimura, S.: Analysis of Crack Propagation and Crack Initiation due to Corrosion of Reinforcement, Construction and Building Materials, Vol. 11, Nos. 7-8, pp.437-442, Dec. 1997

2. Farid Uddin, A.K.M. and Ohtsu, M., BEM Analysis of Mixed-Mode Crack Propagation due to Corrosion of Reinforcement in Concrete, Journal of Materials, Concrete Structures and Pavements, JSCE, No.704/V-55, pp.271-280, May 2002

3. Ohtsu, M. and Yamamoto, T., Compensated Procedure for Half-Cell Potential Measurement, Construction and Building Materials, Vol. 11, Nos. 7-8, pp.398-402, Dec. 1997

4. Chahrour, A.H., and Ohtsu, M., Crack Growth Prediction in Scaled Down Model of Concrete Gravity Dam, Theoretical and Applied Fracture Mechanics, 21, pp. 29-40, 1994

5. Smith, R.N.L. and Mason, J.C., A Boundary Element Method for Curved Crack Problems in Two Dimensions, Boundary Element Methods in Engineering, Springer-Verlag, Berlin, pp.472-484, 1982

6. Erdogan, F. and Sih, G.C., On the Crack Extension in Plates under Plane Loading and Transverse Shear, J. of Basic Eng., No.12, pp.519-527, Dec. 1963

7. Carpinterri, A., Mechanical Damage and Crack Growth in Concrete, Martinus Nijhoff Publishers, Dordrecht, The Netherlands, 1986

8. Farid Uddin, A.K.M. and Ohtsu, M., Application of AE to Fracture Toughness and Crack Analysis by BEM in Concrete, The e-Journal of Nondestructive Testing – ISSN: 1435-4934, Issue Vol.7 No.9, Sep. 2002